CRITICAL BEHAVIOR OF THE DILUTED QUASI-ONE DIMENSIONAL QUANTUM ISING MODEL

by

LOGAN BRADLEY SOWADSKI

A THESIS

Presented to the Graduate Faculty of the

MISSOURI UNIVERSITY OF SCIENCE AND TECHNOLOGY

In Partial Fulfillment of the Requirements for the Degree

MASTER OF SCIENCE

in

PHYSICS

2025

Approved by:

Thomas Vojta, Advisor
Julia Medvedeva
Hyunsoo Kim

PUBLICATION THESIS OPTION

This thesis consists of the following article, formatted in the style used by the Missouri University of Science and Technology.

Paper I: Pages 25-46 are intended for submission to Phys. Rev. B. The manuscript is available here.

ABSTRACT

We explore the phase transition in the diluted quasi-one-dimensional quantum Ising model. We begin by giving an introduction to the Ising model followed by derivations of the properties and observables. A brief overview of Monte-Carlo simulations, is also given focusing on two algorithms that make simulations for physically realizable systems possible, the Metropolis and Wolff algorithms. We finally discuss the concept of random-disorder in the system and the effects this can have on the bulk of the system.

These concepts are then directly applied to a quasi-one-dimensional Ising model. Motivated by recent experiments on the spin-chain material cobalt niobate, we construct a quasi-one-dimensional quantum Ising model with anisotropic spatial interactions. We first consider the classical case. Using Monte Carlo simulations, we study its properties under site dilution.

We then consider the quantum phase transition which is driven by a transverse magnetic field. To do so, we map the transverse-field quantum Ising model to a 4D classical model, which we again study via Monte Carlo simulations.

ACKNOWLEDGMENTS

I would like to begin by thanking my advisor, Dr. Thomas Vojta. His mentorship and instruction have pushed me to new heights as a researcher and student. I would not be where I am today without his guidance.

Thank you as well to Dr. Julia Medvedeva and Dr. Hyunsoo Kim, the members of my thesis committee. Both have provided consultation for me at different periods in this journey, and have been instrumental in the development of this thesis and me as a researcher.

Additionally, I would like to thank my seniors, Ian Heye, Gaurav Khairnar, and Bingjun Shi, who have given invaluable advice over the years.

Finally, I have been supported by an amazing family who have been with me every step of the way. Mother, Father, Ethan, Morgan, and Brooklynn, you have been inspirational to me, and I dedicate this thesis to you.

TABLE OF CONTENTS

Page

PAPER

SECTION

LIST OF ILLUSTRATIONS

LIST OF TABLES

1. INTRODUCTION

Physical systems become greatly more complicated once the number of particles N exceeds 2. For a realistic description of macroscopic systems, N must be increased by several orders of magnitude. Macroscopic systems feature distinct phases (uniform states of matter) and have phase transitions that separate them. In this section, I will introduce the elementary concepts of phase transitions and their applicability in more detail. In this thesis, we are particularly interested in a lattice-bound ferromagnet. Thus I will also introduce the Ising model which is a minimal model that describes the magnetic properties of a lattice-bound uniaxial ferromagnet. I will derive its basic thermodynamic properties through the canonical ensemble and introduce the Monte Carlo algorithms that permit efficient computer simulations. I will finally introduce the concept of random dilution, its representation in an Ising model, and its effects on the phase transitions.

1.1. PHASE TRANSITIONS

A phase transition is constituted by the abrupt change in a macroscopic system's properties when probed by a change of external control parameters. Key properties characterizing phases include, for example, the physical structure, magnetism, and conductivity [1]. Control parameters are related to the external conditions or environment for our system. For example, changes in the temperature, pressure, and magnetic field can cause a system to undergo a phase transition. This is observed in many physical processes in nature including the system we will study in this thesis.

Familiar examples of phase transitions are the changes in the physical structure of water. When the control parameter, temperature T, approaches 0°C from below, the physical lattice structure of water breaks down into a liquid. At 100°C, the liquid undergoes another phase transition to become a gas. These transitions in water are known as 1st-order transitions, characterized by a discontinuous change of the density and by latent heat. A

second example of a phase transition occurs in a ferromagnetic material. Here, a change in the control parameter T leads to a change in its magnetic phase. Above a certain critical temperature T_c, this material will exhibit a paramagnetic phase, which physically corresponds to the magnetic dipoles in the material pointing in random directions. Below T_c the material has a ferromagnetic phase that physically has the magnetic dipoles pointing parallel to one another in the same direction. In contrast to the change in density at the phase transitions of water, the magnetization changes continuously at the ferromagnetic critical temperature, which characterizes a continuous, or 2nd-order transition. Continuous transitions will be discussed in more depth throughout this section and this thesis.

We can better understand the phases of a ferromagnetic system for a given configuration of sites and moments by introducing the magnetic order parameter $\vec{m}$,

$$\vec{m} = \frac{1}{N}\sum_{i=1}^{N}\langle\vec{s}_i\rangle. \tag{1.1}$$

This is defined as the normalized sum of spin vectors over all sites in our system. Here, $\langle\dots\rangle$ denotes the thermodynamic average. When the system is fully ordered, the magnetic moment for all sites will be identical and the sum will take its maximum value. Contrarily, for the fully disordered system, we can expect the value of the spins to be completely random. They thus cancel each other, and the system becomes a paramagnet with $\vec{m} = 0$

1.2. ISING MODEL

The Ising model is a simple mathematical model that can describe ferromagnetic and antiferromagnetic systems [2]. We want to consider, in particular, a system of N sites located on a d-dimensional hypercubic lattice as illustrated in Figure 1.1. Each site is occupied by a spin. We allow these spins to interact with each other. J_{ij} denotes the interaction energy between the spins at sites i and j.

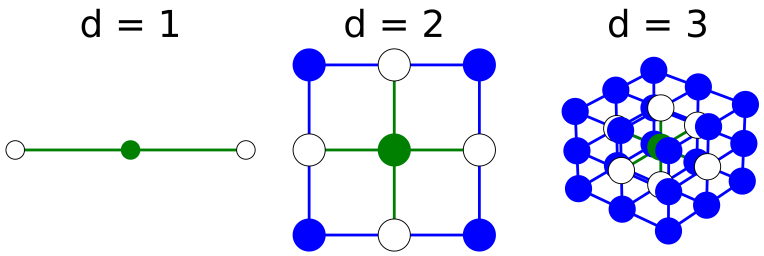

Figure 1.1. Hypercubic lattice for $d = 1, 2, 3$. The principle site is the green dot in the center of each lattice. Unfilled dots are the nearest neighbors to this site. In d dimensions, the number of nearest neighbors is $2d$.

In typical insulating magnets, the interaction strength decreases exponentially with distance [3], allowing us to disregard the interactions from sites that are not nearest neighbors. The Ising model describes the limit of a uniaxial magnet. The spins can therefore be represented by classical variables that take values $\sigma_i = \pm 1$. We can now write the defining Hamiltonian for the Ising model [4] as,

$$H = -\sum_{<ij>} J_{ij}\sigma_i\sigma_j - \mu B \sum_i \sigma_i \tag{1.2}$$

The first term is a summation over all pairs of nearest neighbors. (Figure 1.1 illustrates how the number of nearest neighbors increases, as our system goes to higher dimensions.)

The sign of the interaction J_{ij} distinguishes ferromagnetic and antiferromagnetic systems. For ferromagnets, neighboring spins prefer to be parallel to each other. This means $J_{ij} > 0$ so that the energy is minimized when $\sigma_i = \sigma_j$. Analogously, that for antiferromagnets the interaction, $J_{ij} < 0$, which minimizes the energy when we have anti-parallel spin pairs $\sigma_i = -\sigma_j$. The second term in our Hamiltonian is a summation over all individual sites. This term describes the interaction between the spins and an external magnetic field B. μ is the magnetic moment associated with a spin. In the next sections we will discuss solutions of the Ising model for one and two dimensions. No exact solution exists above two dimensions, but we can obtain approximate results via computer simulations.

1.2.1. One Dimension. The one-dimensional Ising model is known to have an exact solution. We will now summarize this solution and calculate, for later use, some quantities, which are characteristic of one-dimensional magnetic behavior. This behavior is fundamental to understanding weakly coupled spin chains in higher dimensions, as we will see in section 2. Our solution will follow the transfer matrix approach [5] which is simple and has a natural, albeit rigorous, generalization to two dimensions [6]. Consider a one-dimensional Ising chain, as shown for the leftmost structure in Figure 1.1. We enforce periodic boundary conditions (PBC), which effectively turns the chain into a closed loop

$$\sigma_{N+i} = \sigma_i. \tag{1.3}$$

We can then put together the canonical partition function for an Ising chain of N sites,

$$Z = \sum_{\sigma_1=\pm1} \sum_{\sigma_2=\pm1} \sum_{\sigma_3=\pm1} \cdots \sum_{\sigma_N=\pm1} \exp(-\beta H) = \prod_{i}^{N} \sum_{\sigma_i=\pm1} \exp(-\beta H). \tag{1.4}$$

The Hamiltonian of the Ising chain can be written in a symmetric form:

$$H = -J \sum_{i}^{N} \sigma_i \sigma_{i+1} - \frac{\mu B}{2} \sum_{i=1}^{N} (\sigma_i + \sigma_{i+1}), \tag{1.5}$$

where we have assumed a uniform interaction strength between nearest neighbors for all sites. Recall for a moment that $\sigma_i = \pm 1$. We can define matrix elements of an operator $\hat{I}$ via

$$\langle \sigma_i | \hat{I} | \sigma_{i+1} \rangle = \exp(\beta J \sum_{i}^{N} \sigma_i \sigma_{i+1} + \mu B \sum_{i=1}^{N} (\sigma_i + \sigma_{i+1})). \tag{1.6}$$

This 2×2 matrix is known as the transfer matrix. We can express the partition function in terms of the matrix elements as,

$$Z = \sum_{\sigma_i=\pm1} \sum_{\sigma_i=\pm2} \cdots \sum_{\sigma_i=\pm N-1} \sum_{\sigma_i=\pm N} \langle \sigma_1 | \hat{I} | \sigma_2 \rangle \ldots \langle \sigma_{N-1} | \hat{I} | \sigma_N \rangle \langle \sigma_N | \hat{I} | \sigma_1 \rangle$$

$$= \sum_{\sigma_1=\pm 1} \langle \sigma_1 | \hat{I}^N | \sigma_1 \rangle = Tr(\hat{I}^N). \tag{1.7}$$

The trace of this matrix is invariant under a similarity transformation [7]. So, we can express Z in terms of the eigenvalues of $\hat{I}$

$$Z = Tr(\hat{I}^N) = \lambda_1^N + \lambda_2^N. \tag{1.8}$$

We obtain the eigenvalues by solving the eigenvalue equation,

$$\begin{aligned} \det(I - \lambda I) &= \begin{vmatrix} \langle +1|\hat{I}|+1\rangle - \lambda & \langle +1|\hat{I}|-1\rangle \\ \langle -1|\hat{I}|+1\rangle & \langle -1|\hat{I}|-1\rangle - \lambda \end{vmatrix} \\ &= \begin{vmatrix} \exp(\beta(J+)) - \lambda & \exp(-\beta J) \\ \exp(-\beta J) & \exp(\beta(J-)) - \lambda \end{vmatrix} = 0 \end{aligned} \tag{1.9}$$

.

This leads to,

$$\lambda^2 - \lambda \exp(\beta J)(2\cosh(2\mu B\beta)) + 2\sinh(2\beta J) = 0. \tag{1.10}$$

Solving for λ results in,

$$\lambda = \exp(\beta J)\cosh(2\mu B\beta) \pm (\exp(-2\beta J) + \exp(2\beta J)\sinh^2(\mu B\beta))^{1/2}. \tag{1.11}$$

We now have two eigenvalues denoted by λ_1 and λ_2

$$\lambda_1 = \exp(\beta J)\cosh(\mu B\beta) + (\exp(-2\beta J) + \exp(2\beta J)\sinh^2(\mu B\beta))^{1/2}, \tag{1.12}$$

$$\lambda_2 = \exp(\beta J)\cosh(\mu B\beta) - (\exp(-2\beta J) + \exp(2\beta J)\sinh^2(\mu B\beta))^{1/2}. \tag{1.13}$$

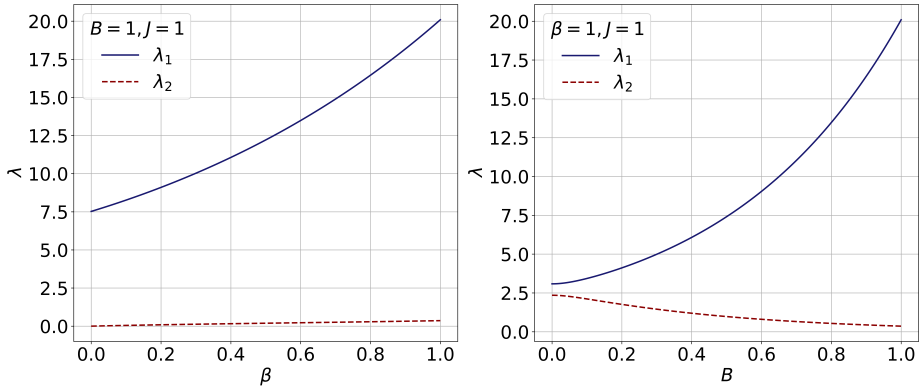

Figure 1.2. Dependence of the eigenvalues λ_1 and λ_2 on the inverse temperature β and external field B. All other parameters are taken to be constant, $B = 1$, $J = 1$ (left) and $\beta = 1$, $J = 1$ (right).

Comparing the two equations, it is clear that $\lambda_1 > \lambda_2$ as can also be seen in Figure 1.2, where we plot λ_1 and λ_2 as functions of the inverse temperature β and external magnetic field B. Both terms in the partition function (1.8) grow exponentially with N. In the thermodynamic limit, as $N \to \infty$, $\frac{\lambda_2^N}{\lambda_1^N} \to 0$. For macroscopic systems, the physical properties will therefore be dominated by λ_1,

$$Z \approx \lambda_1^N. \tag{1.14}$$

From here, calculating thermodynamic quantities is relatively straightforward. Since we are interested in the magnetic properties of this system studying the magnetization is the most advantageous to find the transition temperature.

We start by calculating the Helmholtz free energy F:

$$F(B,T) = \frac{-1}{\beta}\ln(Z), \tag{1.15}$$

$$= -\frac{1}{\beta}\ln[(\exp(\beta J)\cosh(\mu B\beta) + (\exp(-2\beta J) + \exp(2\beta J)\sinh^2(\mu B\beta))^{1/2}]^N,$$

$$= -NJ - \frac{N}{\beta}\ln(\cosh(\mu B\beta) + (\exp(-4\beta J) + \sinh^2(\mu B\beta))^{1/2}). \tag{1.16}$$

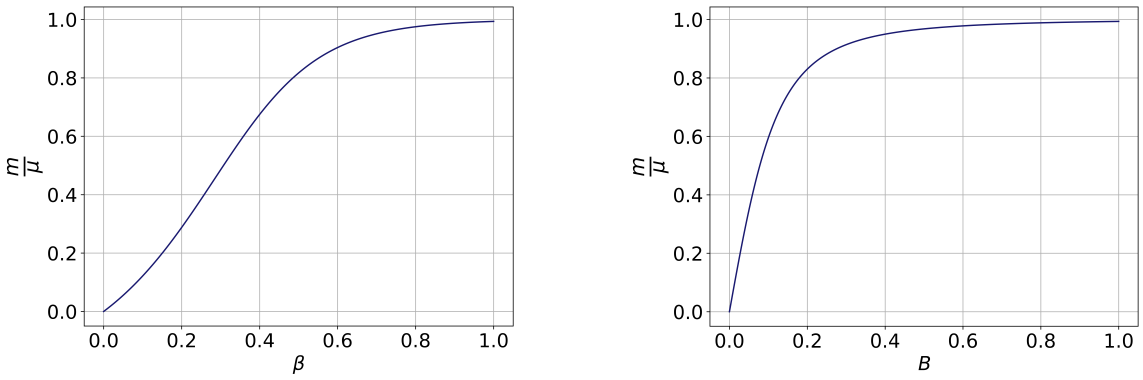

(a) (b)

Figure 1.3. Dependence of the magnetization m on β and B. (a) Magnetization vs. inverse temperature β. $B = 1$ and $J = 1$ are treated as constants. (b) Magnetizations vs. applied field B. $\beta = 1$ and $J = 1$ are treated as constants.

F is related to the magnetization m at constant T,

$$m(B,T) = -\frac{1}{N}\left(\frac{\partial F}{\partial B}\right)_T = \frac{\mu \sinh(\mu B\beta)}{(\exp(-4\beta J) + \sinh^2(\mu B\beta))^{1/2}}. \tag{1.17}$$

Before we calculate the susceptibility we will analyze this magnetization expression. We can infer a lot from this quantity about how the system's magnetic behavior changes with an applied field B and inverse temperature β. Looking at this function illustrated in Figure 1.3, right away we can see as $B \to 0$, for all finite β, $m \to 0$ which indicates that there is no phase transition manifested in the system for finite T. Instead, the system is always in the paramagnetic phase. However if reduce temperature such that $\beta \to \infty$ for all nonzero B, the magnetization takes the value,

$$m_S = \mu, \tag{1.18}$$

where m_S is called the saturation magnetization. This is the maximum magnetization our system can produce and indicates that the system is in a state of perfect order. Thus, there is a transition that has the critical temperature $T_c = 0$! We can now obtain the magnetic

susceptibility from,

$$\chi = \frac{\partial}{\partial B} m = \frac{\partial}{\partial B} \frac{\mu \sinh(\mu B \beta)}{(\exp(-4\beta J) + \sinh^2(\mu B \beta))^{1/2}}. \tag{1.19}$$

$$= \frac{\mu^2 \beta \exp(-4\beta J) \cosh(\mu \beta B)}{(\exp(-4\beta J) + \sinh^2(\mu \beta B))^{3/2}}. \tag{1.20}$$

We are especially interested in the low-field regime in this work, so we let $B \to 0$. We can immediately state $\cosh(2\mu\beta B) \to 1$ and, $\sinh^2(2\mu\beta B) \to 0$. This gives an expression for the temperature dependence of the 'low-field' susceptibility

$$\chi(T) = \frac{\mu^2 \beta \exp(-4\beta J)}{(\exp(-4\beta J))^{3/2}} = \mu^2 \beta \exp(-2\beta J). \tag{1.21}$$

which we will use to characterize the 1D effects we see in more complex systems later in this work. We can see that the zero-temperature transition is also reflected in this quantity by the distinct singularity of χ at $T = 0$.

1.2.2. Two Dimensions. In this section, we will show the exact solution in $d = 2$ (the only other dimension with an exact solution). To visualize this system, instead of a single one-dimensional chain, we can imagine a series of these chains, all connected by additional exchange interactions. If we wrap all of these chains around, like we did for the one-dimensional case, the shape of the two-dimensional case with periodic boundary conditions in both directions appears like a torus. Figure 1.4 illustrates this shape.

We can attack the two-dimensional case with a transfer matrix approach analogous to the one-dimensional case. However, this approach is *very* involved mathematically compared to the one-dimensional case [8]. An exact solution can only be found in zero field. The canonical partition function for the two-dimensional Ising model without field was given exactly first by Onsager [9] and then through the transfer matrix approach by Kaufamn and

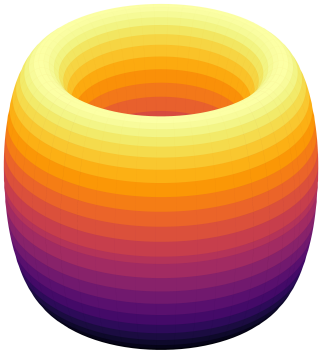

Figure 1.4. A 2D lattice with periodic boundary conditions represented as torus shape.

Onsager [10]. The exact solution for the free energy can be expressed as,

$$-\beta F = \ln(2)+\frac{1}{8\pi^2}\int_0^{2\pi} d\theta_1 \int_0^{2\pi} d\theta_2 \ln[\cosh^2(2\beta J)-\sinh(2\beta J)\cos(\theta_1)-\sinh(2\beta J)\cos(\theta_2)]. \tag{1.22}$$

In contrast to one dimension, this solution features a phase transition at a finite temperature T_c defined by,

$$\sinh^2(2J\beta_c) = 1. \tag{1.23}$$

Solving for T_c yields

$$T_c = 2.269185\frac{J}{K_B}. \tag{1.24}$$

Close to T_c, the behavior of observables in Onsagers solution is governed by power laws. For example, the magnetization behaves as

$$m \sim |T - T_c|^{\beta} \tag{1.25}$$

where $\beta = 1/8$ is the order parameters critical exponent. Analgously, the susceptibility follows the relation

$$\chi \sim |T - T_c|^{-\gamma} \tag{1.26}$$

where $\gamma = 7/4$ is the susceptibility exponent. Similarly, the correlation length scales according to the function

$$\xi \sim |T - T_c|^{-\nu} \tag{1.27}$$

where $\nu = 1$ is the correlation length exponent. This wraps up the analytical solutions that can be obtained for the Ising model. Results for $d > 2$ can only be found via approximate methods or computer simulations such as Monte Carlo simulations. In the next section, we will introduce these methods, and how we can employ them to accurately approximate the behavior of our system.

1.3. MONTE CARLO SIMULATIONS

In higher dimensions, $d > 3$ the Ising model cannot be solved exactly. In this section, we introduce Monte Carlo methods for the Ising model. These methods permit an effective evaluation of thermodynamic quantities as our only limitation becomes computational effort.

According to statistical mechanics, the probability of a particular spin configuration $\vec{\sigma} = (\sigma_1, \ldots, \sigma_N)$ in thermal equilibrium is given by the Boltzmann distribution,

$$P_B(\vec{\sigma}) = \frac{1}{Z} \exp(-\beta H(\vec{\sigma})). \tag{1.28}$$

Now let us consider the average of some generic observable $A(\vec{\sigma})$

$$\langle A(\vec{\sigma}) \rangle_T = \frac{1}{Z} \int \exp(-\beta H(\vec{\sigma})) A(\vec{\sigma}) dx. \tag{1.29}$$

In a Monte Carlo simulation, we replace the sum over all spin configurations, $\vec{\sigma}$ by a sum over a randomly chosen subset of M spin configurations. If the probability of a spin configuration to be in the subset is $P(\vec{\sigma})$, the average of an observable can be written as

$$\langle A(\vec{\sigma})\rangle = \frac{\sum_{l=1}^{M} \exp(-\beta H(\vec{\sigma}_l) A(\vec{\sigma}_l)/P(\vec{\sigma}_l))}{\sum_{l=1}^{M} \exp(-\beta H(\vec{\sigma})/P(\vec{\sigma}))}. \tag{1.30}$$

If we choose $P(\sigma_l)$ to be the Boltzmann probability $P_B(\sigma_l)$, we can see then this expression easily reduces to

$$\langle A(\vec{\sigma}_l)\rangle = \frac{1}{M}\sum_{l=1}^{M} A(\vec{\sigma}_l). \tag{1.31}$$

We are now left with the question of how to generate such a representative subset of spin configurations with the correct Boltzmann probability. In the next section, we will discuss the work of Metropolis and coworkers as well as their algorithm which is instrumental in this thesis. We will then further discuss an algorithm by Wolff that increases our computational efficiency, in addition to a discussion on calculating observables.

1.3.1. Metropolis Algorithm. The Metropolis [11] algorithm is based on the idea of generating the desired subset of spin configurations as a Markov Chain [12]. This means, given a state $\vec{\sigma}_l$ we can construct each successive state, $\vec{\sigma}_{l'}$ based on the previous state and some transition probability. Let us denote the transition probability as $W(\vec{\sigma}_l \to \vec{\sigma}_{l'})$. In the steady state, the probability $P(\vec{\sigma}_l)$ of state $\vec{\sigma}_l$ to appear in the Markov chain fulfills

$$P(\vec{\sigma}_l) W(\sigma_l \to \vec{\sigma}_{l'}) = P(\vec{\sigma}_{l'}) W(\vec{\sigma}_{l'} \to \sigma_l) \tag{1.32}$$

which gives the detailed balance condition,

$$\frac{W(\sigma_l \to \sigma_{l'})}{W(\sigma_{l'} \to \sigma_l)} = \frac{P(\sigma_{l'})}{P(\sigma_l)}. \tag{1.33}$$

If we wish the probabilities $P(\vec{\sigma})$ to be Boltzmann probabilities, this implies

$$\frac{W(\sigma_l \to \sigma_{l'})}{W(\sigma_{l'} \to \sigma_l)} = \frac{\exp(-\beta H(\vec{\sigma_{l'}}))}{\exp(-\beta H(\vec{\sigma_l}))} = \exp(-\beta(H(\vec{\sigma_{l'}}) - H(\vec{\sigma_l}))) = \exp(-\beta(\Delta H)). \quad (1.34)$$

Here ΔH is the change in the Hamiltonian when we update the configuration.

We are now in a position to explicitly describe the steps our Metropolis algorithm takes for a single update of our Ising model, see Table 1.1. Figure 1.5 gives an example of a 2D lattice of sites being indexed by the Metropolis algorithm. To define the transition probabilities, we need to consider two cases for ΔH, $\Delta H \leq 0$ and $\Delta H > 0$. Beginning with the case $\Delta H \leq 0$, the set $W(\vec{\sigma}_l \to \vec{\sigma}_{l'}) = 1$. The reversed update is that where $\Delta H > 0$ such that $W(\sigma_{l'} \to \sigma_l) = \exp(-\beta(\Delta H))$. Our ratio is thus

$$\frac{W[\sigma_l \to \sigma_{l'}]}{W[\sigma_{l'} \to \sigma_l]} = \frac{1}{\exp(\beta(\Delta H)} = \exp(-\beta(\Delta H)) \quad (1.35)$$

as required by the detailed balance condition (1.30)! The Metropolis algorithm is thus a valid Monte Carlo algorithm. However, it becomes inefficient for larger systems at higher dimensions, especially close to the phase transition where the spin configuration contains large chunks of parallel spins. This phenomenon is called critical slowing down. Because of critical slowing down, the number of Monte Carlo sweeps (attempted flips per site) required for equilibration increases very fast, approximately proportional to L^2, close to the phase transition. To overcome the critical slowing down we will now introduce the Wolff algorithm.

Table 1.1. Steps of a single iteration of the Metropolis algorithm.

Step	**Description**
1	**Choose a site:** Select a single site at random with random number generator
2	**Calculate ΔH:** Compute the change in the energy ΔH caused by flipping the spin at the chosen site.
3	**If $\Delta H \leq 0$:** Flip the spin!
4	**If $\Delta H > 0$:** Flip the spin with probability $\exp(-\beta \Delta H)$.
5	**Repeat:** Loop back to step 1 and repeat the procedure.

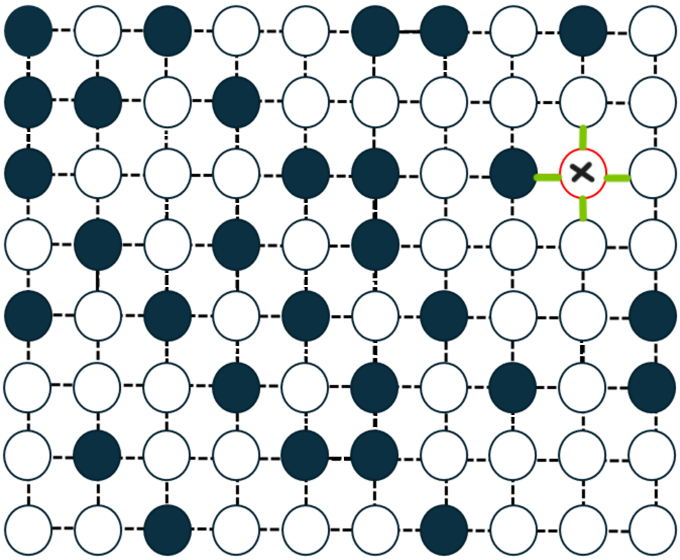

Figure 1.5. 2D lattice illustrating a single Metropolis spin-flip update for a randomly indexed site (x). The nearest neighbors of this site are connected via thick solid lines. The solid dots represent $\sigma_i = +1$, hollow dots (including the chosen site) represent $\sigma_i = -1$.

1.3.2. Wolff Algorithm. The second Monte Carlo algorithm that we employ in this thesis is the Wolff algorithm [13]. This algorithm is still a Markov chain spin-flip algorithm like the Metropolis algorithm. However, rather than flipping individual spins, the Wolff algorithm instead clusters identical spins, reducing the computational cost of our simulations for physically realizable systems. Specifically, it reduces the critical slowing down near the phase transition, which we observe when using the Metropolis algorithm. To derive the Wolff algorithm, we define two types of sites with respect to the site randomly selected as the start site of a cluster. σ_+ sites have a spin value that makes them parallel to the initial site. σ_-, on the other hand, are sites that have a spin value in the opposite direction. The Wolff algorithm iteratively considers the neighbors of sites belonging to the cluster, adjacent σ_+ sites are bonded into the cluster C with probability p_+,

$$p_+ = 1 - \exp(-2\beta J). \tag{1.36}$$

The corresponding bond is defined as an 'accepted' link, Figure 1.6 gives an example of a cluster forming with a set of these links. We denote a given cluster by C and its border by ∂C. The probability that a link between two σ_+ sites will not be activated is given by

$$q_+ = 1 - p_+ = \exp(-2\beta J). \tag{1.37}$$

The complete probability for the construction of the cluster for an update in the configuration is

$$W[\sigma_l \rightarrow \sigma_{l'}] = p_i(\prod_{m_+ \in C} p_+)(\prod_{m_+ \in \partial C} q_+) \tag{1.38}$$

where p_i is the probability of selecting a particular starting site. m_+ counts links between σ_+ sites, while m_- counts links between opposite spins. The reversed update will still involve the same cluster C. It is clear that the probability p_i will be the same in both cases. We can write out the reversed probability for the reversed update as

$$W[\sigma_{l'} \rightarrow \sigma_l] = p_i(\prod_{m_+ \in C'} p_+)(\prod_{m_+ \in \partial C'} q_+). \tag{1.39}$$

Table 1.2. Steps of a single iteration of the Wolff algorithm.

Step	Description
1	**Choose a site:** Select a single seed site at random with random number generator
2	**Construct cluster:** Consider all nearest neighbors connected to initial site. If a neighbor spin is parallel to the seed spin, add to cluster with probability $p_+ = 1 - \exp(-2\beta)$
3	**Continue construction:** Consider the set of sites added in the previous update. Repeat step 2 for each of these sites.
4	**Further continue construction:** Continuously apply step 3 for each subsequent update until no new sites are added by the update.
5	**Flip and Repeat:** Flip entire cluster and proceed back to step 1 to construct a new cluster.

We can write the ratios of these probabilities as

$$\frac{W[\sigma_l \to \sigma_{l'}]}{W[\sigma_{l'} \to \sigma_l]} = \frac{(\prod_{m_+ \in C} p_+)(\prod_{m_+ \in \partial C} q_+)}{(\prod_{m'_+ \in C'} p_+)(\prod_{m'_+ \in \partial C'} q_+)}. \tag{1.40}$$

Viewing Figure 1.6 can help visualize the two updates we're discussing. The m_+ links making up the internal part of the cluster C, will be the same exact m_+ links making up the internals of the updated cluster C'. This makes our products of probability p_+ equal for both clusters so that our ratio becomes

$$\frac{W[\sigma_l \to \sigma_{l'}]}{W[\sigma_{l'} \to \sigma_l]} = \frac{(\prod_{m_+ \in \partial C} q_+)}{(\prod_{m'_+ \in \partial C'} q_+)} = \frac{\exp(-2\beta J N_+)}{\exp(-2\beta J N'_+)} \tag{1.41}$$

where N_+ denotes the number of m_+ border links. However, for the border of our cluster ∂C, the links m_+ are instead the links m_- for the updated cluster $\partial C'$. We can write this mathematically as

$$\begin{aligned} \exp(-\beta J N_+) &= \exp(\beta J N'_-) \\ \exp(-\beta J N'_+) &= \exp(\beta J N_-). \end{aligned} \tag{1.42}$$

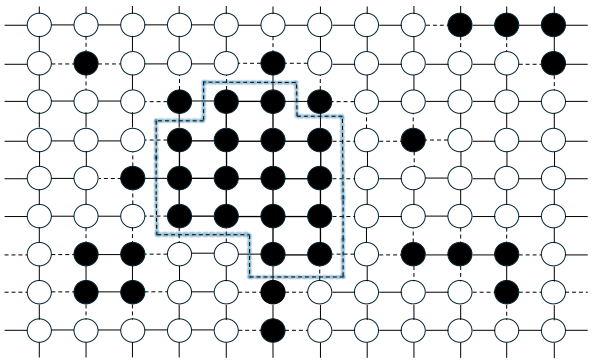

Figure 1.6. Wolff algorithm cluster formation example where all links are activated. Accepted links are bolded and encapsulated by the highlighted dotted line which form the cluster.

This allows us to write the ratio as

$$\begin{aligned}\frac{W[\sigma_l \to \sigma_{l'}]}{W[\sigma_{l'} \to \sigma_l]} &= \frac{\exp(-\beta J N_+)\exp(-\beta J N_+)}{\exp(-\beta J N'_+)\exp(-\beta N'_+)} \\ &= \frac{\exp(-\beta J N_+)\exp(\beta J N'_-)}{\exp(-\beta J N'_+)\exp(\beta J N_-)} \\ &= \frac{\exp(\beta J N'_+)\exp(\beta J N'_-)}{\exp(\beta J N_+)\exp(\beta J N_-)} \\ &= \frac{\exp(\beta J N')}{\exp(\beta J N)}.\end{aligned} \tag{1.43}$$

The contribution of the boundary sites to the total energy is $H(\sigma_l) = -JN$. Applying this, we obtain the same condition for the ratio of probabilities for the Metropolis case

$$\frac{W[\sigma_l \to \sigma_{l'}]}{W[\sigma_{l'} \to \sigma_l]} = \exp(-\beta \Delta H). \tag{1.44}$$

The update and reversed update both flip the same exact internal sites with one another which is what makes the above result possible. The only changes between these two updates will be exclusively at the boundary links for each cluster. Thus, the Wolff algorithm fulfills the detailed balance condition (1.33) and is thus a valid Monte Carlo algorithm. The Wolff algorithm greatly improves the critical slowing down, the required number of sweeps is only weakly dependent on system size.

1.3.3. Numerical Results for Higher Dimensional Ising Model. The 3D Ising model has yet to be solved exactly [8]. However, we can study it, along with lower-dimensional models using Monte Carlo Simulations. Different from the 2D case, which can be defined on a $L_x \times L_y$ square lattice, the 3D case can be defined on a cubic lattice with dimensions $L_x \times L_y \times L_z$. Consequently, the number of nearest neighbors for a given site has also increased from 4 to 6. Unlike the 1D and 2D cases, the periodic boundary conditions are not as simple to visualize through a 'chain' or 'torus'. This does not mean we can not enforce them, though, and it is easiest to express it mathematically. Denoting the spin m coordinates x, y, z by $\sigma(x, y, z)$, the periodic boundary conditions read $\sigma(x + L_x, y, z) = \sigma(x, y, z)$ and

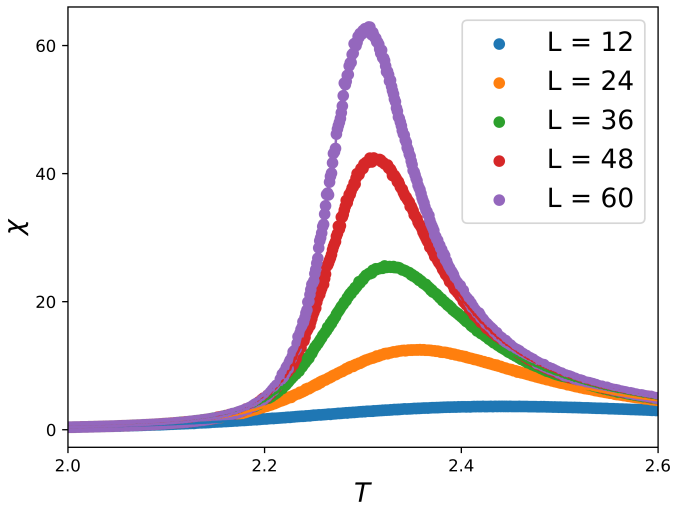

Figure 1.7. Susceptibility of the 2D Ising model as a function of temperature for different system sizes L, diverging at $T_c \approx 2.27$, in agreement with Onsagers value $T_c \approx 2.269$ [9].

analogous for the other directions. Here L_x is the linear system size in the x direction. We will now make use of the methods introduced, and implement the Metropolis algorithm to generate the necessary distribution of spins we need to accurately characterize the system. We investigate observables related to the magnetization to determine when a phase transition takes place. Specifically, we will calculate the susceptibility which can be expressed as

$$\chi = \frac{\partial m}{\partial B} = N\beta(\langle m^2 \rangle - \langle m \rangle^2) \tag{1.45}$$

where m is the magnetization of a particular spin configuration,

$$m([\sigma]) = \frac{1}{N}\sum_i \sigma_i. \tag{1.46}$$

The susceptibility, which is a response quantity, contains the variance of the magnetization values calculated within the system. This is an example of the fluctuation-response theorem. The fluctuations in the magnetization increase as the system approaches T_c. This causes χ to diverge towards infinity at T_c in the thermodynamic limit. This is illustrated in Figure 1.7

which shows χ vs T for the 2D Ising model, for $L_x = L_y = L = 12, 24, 36, 48, 60$. As we can see, right at the calculated T_c in equation (1.24), the susceptibility has a strong peak whose maximum diverges towards infinity for system sizes $L \to \infty$. More precisely, the peak position $T_{\max}$ approaches T_c in the thermodynamic limit $N \to \infty$. One can thus use an extrapolation of $T_{\max}$ to infinite system size to find T_c.

An additional useful quantity in our simulations, is the Binder cumulant which is a tool towards identifying second order phase transitions. It is defined as [12]

$$g = \left[1 - \frac{\langle |m|^4 \rangle}{3\langle |m|^2 \rangle^2}\right]_{dis}. \tag{1.47}$$

The second term contains the ratio of the fourth moment of the magnetization and the second moment squared. This is designed to focus on the fluctuations of our system which gives this quantity the power to identify T_c by identifying scale-invariant fluctuations that are unique to the system at the critical temperature. Above T_c in the paramagnetic phase, the system contains many independently fluctuating spins. The distribution of m is thus, a Gaussian centered at zero. This implies $\langle m^4 \rangle = 3\langle m^2 \rangle^2$ and $g = 0$ in the thermodynamic limit. Below T_c in the ordered phase, the system is magnetic and $\langle m^4 \rangle \approx \langle m^2 \rangle^2 \approx 1$. The value of the Binder cumulant therefore takes the maximum value, $g = 2/3$ in the thermodynamic limit. At T_c however, g captures the critical fluctuations, which are scale-invariant i.e, independent of L. Thus by plotting the Binder cumulant as a function of temperature, for a variety of system sizes L^3, we can obtain T_c by identifying the point where all systems have the same value of g.

The Binder cumulant crossing is illustrated in Figure 1.8 for a set of sizes, $L = 12, 24, 36, 48$. As explained previously, T_c will be the temperature value where g is identical for all system sizes. This is found in our case to be a temperature of about 4.51, in agreement with literature values[9].

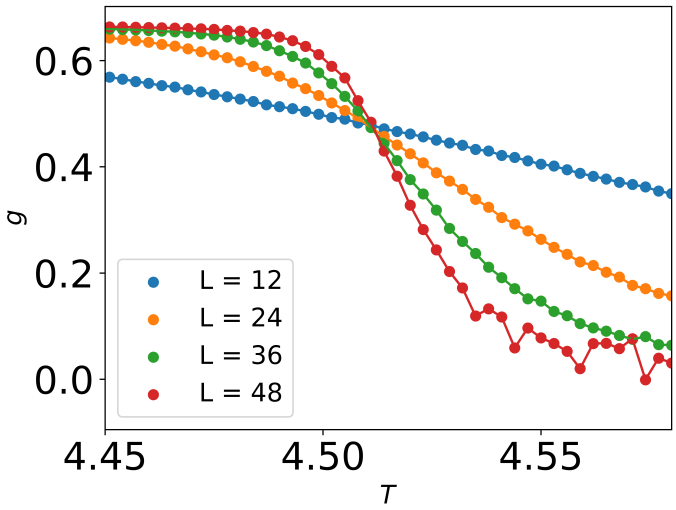

Figure 1.8. Binder cumulant for 3D Ising model as a function of temperature for different system sizes L. The curves for different L cross at $T \approx 4.51$ which gives an estimate of T_c.

1.4. QUENCHED DISORDER

So far, we have established the underpinning for the Ising model and how to obtain its thermodynamics via numerical simulations. We have treated all sites identically with no defects or disorder. In experiments, it is notoriously difficult to obtain or create a perfectly pure system, even in extremely controlled environments. Physically realizable systems often have some degree of disorder as a result of defects that can form in their creation. Defects in the atomic positions or species of a sample are common examples that can cause disorder and influence the macroscopic properties of the system. In solids, the defects are usually time-independent over the time span of an experiment. The 'frozen' nature of the defects in the system is what gives this form of disorder the name 'quenched' disorder. In this section, we will implement quenched disorder in the Ising model. We look to answer the question, how does quenched disorder affect the phase transition of an Ising model?

1.4.1. Diluted Ising Model. One important type of quenched disorder is site dilution in which vacancies or non-magnetic atoms randomly replace magnetic atoms. The strength of the dilution can be characterized by an impurity concentration $p = N_{\text{imp}}/N$ where

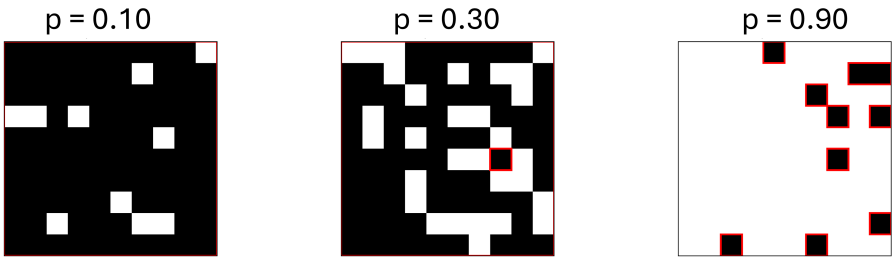

Figure 1.9. 2D lattice with site dilution. Filled boxes are magnetic sites. Empty boxes are vacancies. Clusters of spins isolated from the system by impurities are highlighted in red (color). Examples are shown for three dilutions (from left) $p = 0.10, 0.30, 0.90$

N_{imp} is the number of impurities and N is the total number of lattice sites. Creating a system with a particular impurity concentration can be as simple as randomly placing vacancies around the lattice with probability p. Figure 1.9 displays examples of a two-dimensional lattice with site dilution for different p.

The diluted form of the Ising model Hamiltonian is a deceptively simple modification of the Ising model introduced previously. The Hamiltonian reads

$$H = -\sum_{<ij>} J_{ij}\epsilon_i\epsilon_j\sigma_i\sigma_j \tag{1.48}$$

where the only addition are the quenched random variables ϵ_i. ϵ_i decides whether to make a site an impurity ($\epsilon_i = 0$) or a magnetic site ($\epsilon_i = 1$).

In the simplest case we can independently assign an impurity to each site with probability (concentration parameter) p. This is the definition of "uniform random site dilution". Uniform random vacancy placement is an assumption and may not accurately describe the system. For some magnetic systems, it is known that the vacancy distribution is strongly non-uniform [14]. We do not consider such cases in this thesis, and limit our discussion of dilution to that of perfectly uniform random site dilution.

In the presence of random site dilution, the exact impurity positions vary from sample to sample. The physical properties of two (finite-size) samples are thus different, even if they have the same impurity concentration. In the thermodynamic limit, physical properties are expected to be self-averaging. They are therefore best represented by an ensemble average over many disorder configurations. The number of configurations needed in computer simulations depends on the details of the system and on the strength of the disorder-influenced fluctuations. This can be monitored via the variance of appropriate observables.

1.4.2. Percolation and Magnetic Phase Boundary. Placing vacancies within our system reduces the magnetic interactions of a given site and therefore suppresses the tendency towards magnetic order. However, the system remains ferromagnetic at the lowest temperatures until the vacancy concentration reaches a critical value p_c, where there are so many vacancies in the system that it is no longer possible to construct a connected cluster of magnetic sites that spans the entire system (as in the rightmost case in Figure 1.9). This in turn means that the system can no longer maintain long-range magnetic order. The complement of this critical value (i.e, the minimum concentration of magnetic sites) is called the percolation threshold $P_c = 1 - p_i$. We use capital P to denote the concentration of occupied sites and p to denote the concentration of vacancies. For a system where $P \geq P_c$, the system can still maintain order and exhibit ferromagnetic behavior. Once $P < P_c$, the system features only finite-size clusters, destroying long-range order and making the system exhibit paramagnetic behavior. We can expect our system to have the highest transition temperature when no magnetic sites are removed (i.e for $T_c \rightarrow T_{c-max}$ $P \rightarrow 1$). In contrast, for $P \rightarrow P_c$, $T_c \rightarrow 0$. How does the critical temperature T_c, change as the impurity concentration is increased from 0 to p_c? Since we have already put together a working numerical solution of the 3D Ising model, it is opportunistic to implement dilution into the program there and study directly the effect on the phase boundary $T_c(p)$. Random site dilution, where the diluted sites are treated as vacancies, can be easily implemented by

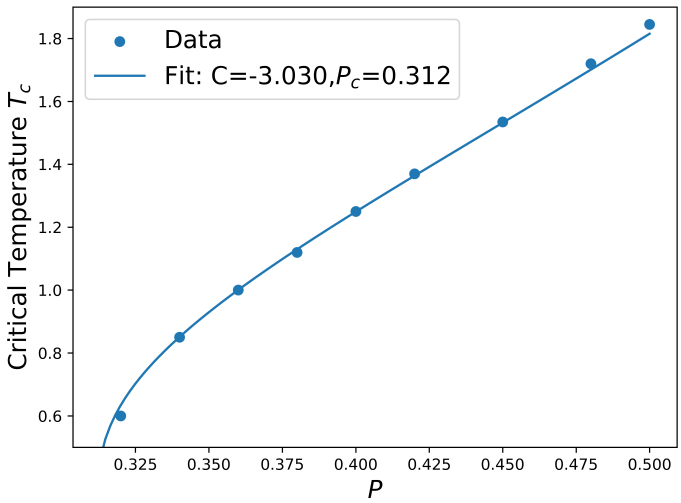

Figure 1.10. Magnetic phase boundary for diluted 3D Ising model on a cubic lattice with PBC. Dots represent the calculated data, line is a fit to the function $T_c = \frac{C}{ln|p-p_c|}$.

means of a random number generator. It is an iterative procedure to construct the phase boundary within our simulations. We consider a set of impurity concentrations between zero and the percolation threshold $p_c = 1 - P_c$, where we expect $T_c = 0$. The percolation threshold of a simple cubic lattice is $P_c = 0.3116077(3)$ [15]. We consider the following set of dilutions in the simulations

$$p_i = [0, 0.1, 0.2, 0.3, 0.4, 0.5, 0.6, 0.62, 0.64, 0.66, 0.68, 0.70]. \tag{1.49}$$

$p = 0$ is the clean, impurity-free system we have already simulated in a previous section. Considering each concentration p, we run a series of Monte Carlo simulations that determine the critical temperature. The results are detailed in Figure 1.10. Close to the percolation threshold, the dependence of the T_c on p is of logarithmic type, [16]

$$T_c = \frac{C}{\ln(p - p_c)}. \tag{1.50}$$

1.4.3. Harris Criterion. We have seen that disorder can change the transition temperature of a phase transition. Can it also change universal properties such as the critical exponents? This question was answered by Harris [17] who discovered the inequality that describes the stability of a critical point in the clean system against disorder. It reads,

$$\nu d > 2 \tag{1.51}$$

where d is the spatial dimensionality and ν is the critical exponent describing the divergence of the magnetic correlation length $\xi \simeq |T - T_c|^{-\nu}$ [1]. Harris derived this criterion by considering the variations of the local critical temperature from region to region in the sample. When these variations are large, it leads to some regions being in the paramagnetic phase and others being in the ferromagnetic phase. This makes a uniform transition temperature for the system impossible [17]. Harris found that the strength of the local T_c variations diverges as the critical point is approached if the criterion is violated such that $\nu < \frac{2}{d}$. However, if the Harris criterion is fulfilled, $\nu > \frac{2}{d}$, the system becomes less disordered as the critical point is approached. The thermodynamic observables are self-averaging, and the critical behavior is the same as for the clean system [18].

1.4.4. Quantum (Transverse-field) Ising Model. So far, we have primarily focused on classical phase transitions, where the critical point is driven by a change in temperature. However, phase transitions can also occur at absolute zero temperature ($T = 0$). These zero-temperature transitions are known as quantum phase transitions, and are driven by changes to other parameters, for example, pressure and magnetic field. A prototypical example of a model with such a transition is the transverse-field Ising model, given by the Hamiltonian,

$$H = -J \sum_{\langle i,j \rangle} \sigma_i^z \sigma_j^z - h \sum_i \sigma_i^x \tag{1.52}$$

[1] The correlation length ξ characterizes the decay of the spin-spin correlation function with distance $\langle S_i S_j \rangle - \langle S_i \rangle \langle S_j \rangle \sim \exp(r_{ij}/\xi)$

where σ_i^z and σ_i^x are Pauli matrices that represent the components of the spin operator at site i. The J term favors ferromagnetism, while the transverse field h induces quantum fluctuations. This follows because the Pauli matrix σ_i^x can be decomposed into the spin-flip operators $\sigma_i^x = \sigma_i^+ + \sigma_i^-$. Thus when the site interaction strength J dominates relative to h (i.e. $J \gg h$), the system favors a ferromagnetic ground state. In contrast, when $h \gg J$, the transverse magnetic field disrupts the alignment of spins causing the system to have a paramagnetic ground state.

Disorder effects at quantum phase transitions are generically stronger than those of classical transitions [18, 19]. This has been shown, for example, for the one-dimensional random transverse field Ising chain, with the Hamiltonian

$$H = -\sum_i J_i \sigma_i^z \sigma_{i+1}^z - \sum_i h_i \sigma_i^x \tag{1.53}$$

where J_i and h_i are random variables. Fisher [20] used a strong-disorder renormalization group approach to investigate the quantum phase transition in this problem, showing that it is of exotic infinite-randomness type. Unlike conventional critical points, observable distributions (e.g., correlations) broaden without bound in the thermodynamic limit. In such models, observables follow power laws (e.g., susceptibility, correlation length). However, at an infinite-randomness point, the dynamical scaling is governed by activated scaling, featuring an exponential relationship between correlation time and correlation length, $\ln(\xi_\tau) \sim \xi^\psi$ where ψ is the so-called tunneling exponent. For the 1D transverse-field Ising model, ψ takes the value $1/2$. At a conventional critical point, the dynamical scaling is of power-law type instead, $\xi_\tau \sim \xi^z$, where z is the dynamical exponent. This behavior change is a dramatic shift from the scaling laws and behavior that are characteristic of the classical Ising model.

PAPER

I. QUANTUM CRITICAL BEHAVIOR OF DILUTED QUASI-1D ISING CHAINS

Logan Sowadski and Thomas Vojta
Department of Physics
Missouri University of Science and Technology
Rolla, Missouri 65409–0050
Tel: 573–341–6622, Fax: 573–341–4115
Email: logansowadski@mst.edu

ABSTRACT

$CoNb_2O_6$ is a unique magnetic material. Its quantum critical behavior has been shown to belong to the one-dimensional transverse-field Ising universality class. This behavior is facilitated by the structural arrangement of magnetic Co^{2+} ions in nearly isolated zig-zag chains. In this work, we investigate the effect of random magnetic site dilution on the critical properties of this system. To this end, we develop an anisotropic site-diluted 3D transverse-field Ising model. We find that the disorder leads to unconventional activated scaling behavior at the quantum critical point. Interestingly, the critical exponents of the quantum phase transition are in good agreement with those of the disordered 3D transverse-field Ising model, despite the strong spatial anisotropy.

Keywords: Cobalt Niobate, Quantum Phase Transition, Infinite Randomness, Disordered Ising Model

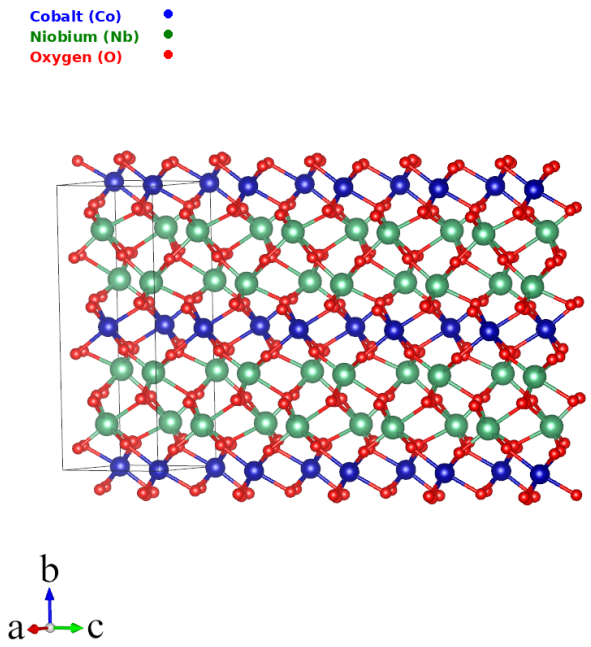

Figure 1. Crystal Structure of $CoNb_2O_6$. Atom positions taken from [1].

1. INTRODUCTION

Recent years have seen several interesting studies of the magnetic material cobalt niobate, $CoNb_2O_6$. The material orders magnetically below about 3K. At the lowest temperatures, it undergoes a quantum phase transition (QPT) as a function of a magnetic field applied along the crystallographic *b*-axis [2]. An intriguing result from these experimental studies is that the critical behavior of the QPT is well described by the one-dimensional transverse-field Ising model (TFIM). This alignment of nature and theory is a result of $CoNb_2O_6$s fascinating crystal structure [3]. $CoNb_2O_6$ forms in a columbite structure as shown in Figure 1. The magnetic Co^{2+} ions have an effective moment of spin-1/2, and are embedded within a three-dimensional lattice of NbO_6 octahedrals. Along the *c* direction, the Co^{2+} atoms have strong magnetic interactions with one another and form well-coupled, zig-zagging chains of magnetic sites. These 'one-dimensional' chains are coupled to one

another in the system via weak inter-chain interactions. Magnetization measurements and neutron scattering experiments showed the exchange interactions in these weak directions, are about 10-50 times weaker than those along the strongly coupled chains [2, 4]. Thus, we assume that these weak couplings have a relatively small influence on the critical behavior of the pure system, confirmed by the one-dimensional TFIM universality class observed experimentally [2]. More recent investigations into cobalt niobate have shown that its magnetic behavior is considerably more complicated. In a conventional TFIM, the ferromagnetic state features two degenerate ground states with static domain walls at zero field. However, terahertz spectroscopy experiments have shown that for $CoNb_2O_6$, the domain wall are already mobile even with no transverse magnetic field applied [5]. This 'quantum motion' of the domain walls does not fit with the TFIM framework proposed before, and reflect additional complications to the magnetic behavior. It has therefore been proposed that even though the quantum critical behavior is well described by the 1D TFIM universality class, the complete magnetic properties are better described by a twisted Kitaev chain [5].

In this work, we investigate the effects of quenched disorder on the QPT in this system. Specifically, we consider site dilution via the substitution of magnetic Co^{2+} with vacancies or non-magnetic atoms. The insertion of such vacancies greatly challenges the formation of long-range magnetic order in the system. For the pure system without vacancies, magnetic correlations can be established with relative ease along the chains of magnetic ions in the *c* direction. A weak inter-chain coupling is then sufficient to produce long-range order. However, the substitution of magnetic sites with non-magnetic ones 'breaks' the strongly-coupled chains, forcing the system to rely on the significantly weaker inter-chain interactions to reach long-range magnetic order, greatly complicating the magnetic interactions at play.

To model this physical situation and its effect on the quantum phase transition, we propose a disordered quasi-one-dimensional TFIM. This is constructed from a three-dimensional TFIM, where spatially anisotropic interactions and site dilution are implemented.

We then map the quantum Hamiltonian onto an anisotropic 4D classical Ising model with columnar disorder. Monte Carlo methods that make use of cluster algorithms are used to perform the calculations and finite-size scaling techniques are used for the data analysis. Specifically, we study the unconventional scaling behavior of this quantum phase transition due to the presence of site dilution and demonstrate that it belongs to the disordered three-dimensional TFIM universality class, despite the strong spatial anisotropy of the Hamiltonian.

2. MODEL

Experimental observations have found that the QPT of pure cobalt niobate is well described by the one-dimensional TFIM. As discussed in section 1, the presence of site dilution makes incorporating weak inter-chain couplings into the model crucial, as magnetic long-range order is impossible otherwise. Thus we begin by defining the Hamiltonian for the 3D anisotropic site-diluted TFIM on a cubic lattice [6],

$$H = -\bar{J}_s \sum_{\langle i,j\rangle_s} \epsilon_i \epsilon_j \sigma_i^z \sigma_j^z - \bar{J}_\perp \sum_{\langle i,j\rangle_\perp} \epsilon_i \epsilon_j \sigma_i^z \sigma_j^z - B \sum_i \epsilon_i \sigma_i^x. \tag{1}$$

The first term represents interactions between nearest neighbors along the strong chain, indexed by $\langle i, j\rangle_s$, with an interaction strength $\bar{J}_s$. The z-component Pauli matrices σ_i^z govern the spin interactions between sites on this chain. The second term accounts for interactions in the two spatial directions perpendicular to the chains, indexed by $\langle i, j\rangle_\perp$. These sites are linked by the interaction strength $\bar{J}_\perp$. The ratio $\bar{J}_\perp/\bar{J}_s$ tunes the anisotropy of interactions in the system. In order to properly incorporate the physics of cobalt niobate, $\bar{J}_\perp$ must be chosen to be sufficiently weak, such that $\bar{J}_s \gg \bar{J}_\perp$. We will return to the values of $\bar{J}_s$ and $\bar{J}_\perp$ in a later section. The third term represents the transverse field B, which affects all sites uniformly and couples to the x-component Pauli matrices σ_i^x. These operators can be decomposed as $\sigma_i^x = \sigma_i^+ + \sigma_i^-$, corresponding to spin-flip operators that toggle between

spin-up and spin-down states. Quantum fluctuations introduced by the transverse field B can thus disrupt the long-range ferromagnetic order in the system when the field strength reaches a critical threshold B_c. This threshold is the quantum critical point which is studied in this work. Finally, ϵ_i is a quenched random variable that accounts for site dilution. It takes a value 1 for a magnetic site with probability $1 - p$, and 0 for a substituted vacancy with probability p. Note that we do not include the more complicated interactions discussed in Ref. [5] as they are not expected to affect the critical behavior.

2.1 QUANTUM TO CLASSICAL MAPPING

Our computer simulations of this quantum system can be simplified by mapping the Hamiltonian to an equivalent classical model. This allows us to use classical Monte Carlo cluster algorithms that require considerably less numerical effort. Mapping the quantum 3D TFIM to a classical model involves extending the dimensionality of the system. According to the quantum-classical correspondence, the thermodynamic behavior of a d-dimensional quantum system can be mapped to that of a $(d + 1)$-dimensional classical system [7]. Thus, we map the 3D TFIM (1) to a 4D classical Ising model on a hypercubic lattice. This system has 3 spatial dimensions that correspond to the single strongly-coupled direction labeled by s and two weakly coupled directions labeled by $\perp$. The fourth dimension represents imaginary time τ [8]. The 4D classical Ising model Hamiltonian reads

$$H = -J_s \sum_{\langle i,j\rangle_s,\tau} \epsilon_i\epsilon_j S_{i,\tau}S_{j,\tau} - J_\perp \sum_{\langle i,j\rangle_\perp,\tau} \epsilon_i\epsilon_j S_{i,\tau}S_{j,\tau} - J_\tau \sum_{i,\tau} \epsilon_i S_{i,\tau}S_{i,(\tau+1)}. \qquad (2)$$

Here i and j denote spatial lattice sites, and τ is the imaginary time coordinate. The first term considers the couplings in the strong spatial direction, indexed by $\langle i, j\rangle_s$, with an interaction strength J_s. The second term contains the interactions in the weak spatial directions, and the last term is the interaction in the imaginary time direction. $S_{i,\tau}$ indicates the classical Ising spin at each remaining magnetic site. Geometrically, the anisotropic $3D$ quantum

system of size $L_s \times L_\perp^2$ can be mapped to that of the hypercubic $4D$ classical system of size $= L_s \times L_\perp^2 \times L_\tau$. Here, L_s is the length of the strongly coupled chains. Similarly, $L_\perp$ is the system size in the two weak spatial directions. L_τ is the site in the imaginary time direction. The interactions J_s and $J_\perp$ in the classical Hamiltonian are related to $\bar{J}_s$, $\bar{J}_\perp$ of the quantum model (1). Analogously, the value of the imaginary-time interaction J_τ is determined by the transverse-field strength B. As we are interested in the universal properties of the phase transition, the exact values are unimportant. We therefore fix $J_s = J_\tau = 1$ and use $J_\perp$ to control the spatial anisotropy. The transition is tuned via the temperature of the classical model, T_{eff}. It differs for the temperature of the original quantum model, which remains at zero [7].

2.2 SITE DILUTION

Quenched disorder is implemented as site dilution by substituting magnetic sites for non-magnetic vacancies. This is delivered via the independent quenched random variables ϵ_i. They take the values 0 (vacancy) with probability p and 1 (magnetic site) with probability $1 - p$. Thus, the value p indicates the concentration of the vacancies. As the vacancy positions are independent of time, the disorder is columnar, i.e, perfectly correlated in the imaginary time direction. The simulations shown in this work are taken at a value of $p = 0.10$, effectively substituting 10% of magnetic sites with vacancies. This relatively small value for p is chosen, to allow the strongly coupled magnetic sites to still form chains of a significant length. This, in principle, permits observables to feature one-dimensional behavior, at least in a transient regime (as observed in the experiment on the clean compound [2]).

2.3 CLASSICAL TEST

In addition to the quantum model discussed above, we prepare a classical model to study the effects of increased anisotropy on the correlations between the strongly coupled chains in the system. For the analysis of these effects, we employ a classical, 3D, anisotropic, site-diluted Ising Hamiltonian,

$$H = -J_s \sum_{\langle i,j \rangle_s} \epsilon_i \epsilon_j S_i S_j - J_\perp \sum_{\langle i,j \rangle_\perp} \epsilon_i \epsilon_j S_i S_j. \tag{3}$$

It takes a similar form to (2), where the only difference is the removal of the imaginary time direction τ, and the corresponding interactions. To test the effects of anisotropy on this system, we consider increasingly large ratio $J_s/J_\perp$ and consider their effects on the magnetic correlations. This analysis is presented in a later section.

3. MONTE CARLO SIMULATIONS

3.1 ALGORITHM

The computer simulations reported in this paper have been performed by employing large-scale Monte Carlo simulations of the mapped classical Ising model (2). The appropriate choice of algorithm is paramount for the efficiency of the simulations. We utilize a hybrid approach, combining the Wolff cluster [9] and Metropolis single-spin flip [10] algorithms. The Wolff algorithm greatly reduces the critical slowing down of the system near criticality and enables us to study larger systems at a reasonable computational cost. However, in the presence of site dilution, the Wolff algorithm alone is insufficient, as it may fail to update small, isolated spin clusters that are disconnected from the main lattice. To address this, we pair this algorithm with Metropolis single-spin updates which consider all sites, including those disconnected from the main lattice. Thus, a full Monte Carlo sweep consists of one

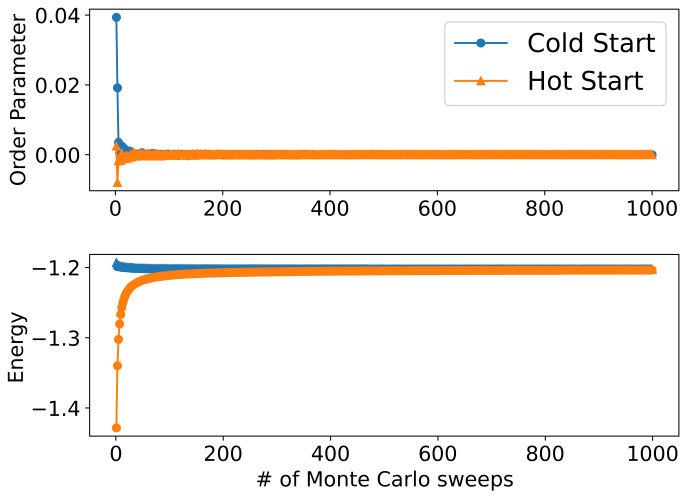

Figure 2. Order parameter and Energy versus the number of Monte Carlo sweeps for a single sample. Mapped classical system evaluated with optimal geometry: $L_\tau^{max} = 3080 = 11L_s = 440L_\perp$. $J_s = J_\tau = 100J_\perp$, $T = 2.22$.

Wolff cluster sweep [9] followed by one Metropolis sweep over the lattice [10]. This two-step approach ensures that all regions of the lattice, including isolated clusters, are adequately equilibrated, thereby achieving more accurate results.

3.2 EQUILIBRATION AND MEASUREMENT

The simulation process begins with an equilibration phase, where the system undergoes a series of sweeps until it reaches a steady state. We establish an equilibration threshold by comparing runs employing hot starts (random initial spin configurations) and cold starts (all spins aligned). Figure 2 illustrates the equilibration process, by showing the order parameter m and energy E versus the number of Monte Carlo sweeps. When values from both starting conditions converge and remain stable, the system is considered equilibrated.

For the 3D classical case, the system equilibrates after approximately 300 sweeps , while for the quantum case mapped to a 4D Ising model, 500 sweeps are required due to the additional complexity introduced by quantum fluctuations. Both of these values are obtained

for the maximum system size considered in this study. Based on these observations, we perform 1000 equilibration sweeps followed by 500 measurement sweeps in the production runs with measurements taken after each (measurement) sweep.

The quenched disorder creates additional sample-to-sample variations of the results in our system. To suppress the disorder fluctuations, all physical quantities are averaged over 2000 to 20, 000 independent disorder configurations for each system size. Statistical errors of the observables are obtained from the statistics of the sample-to-sample fluctuations. Simulating a large number of disorder configurations using relatively short Monte-Carlo runs has been shown to reduce the overall statistical error for a given numerical effort [11].

3.3 DATA ANALYSIS

A variety of observables are considered in this paper to investigate the critical behavior of the system. The order parameter m is defined as,

$$m = \frac{1}{N_{\mathrm{mag}}} \sum_{i,\tau} \epsilon_i S_{i,\tau}. \tag{4}$$

Here, N_{mag} is the number of magnetic sites and N_{imp} is the number of impurities from site dilution. They fulfill $N = N_{\mathrm{mag}} + N_{\mathrm{imp}}$ where N is the total number of sites. The susceptibility χ is given by,

$$\chi = [N_{\mathrm{mag}}\beta(\langle m^2\rangle - \langle m\rangle^2)]_{dis} \tag{5}$$

where $\langle \dots \rangle$ indicates the thermodynamic average over the Monte Carlo measurement sweeps. $[\dots]_{\mathrm{dis}}$ denotes the average over the disorder configurations considered. The susceptibility is expected to diverge at the critical point, an indication of a phase change.

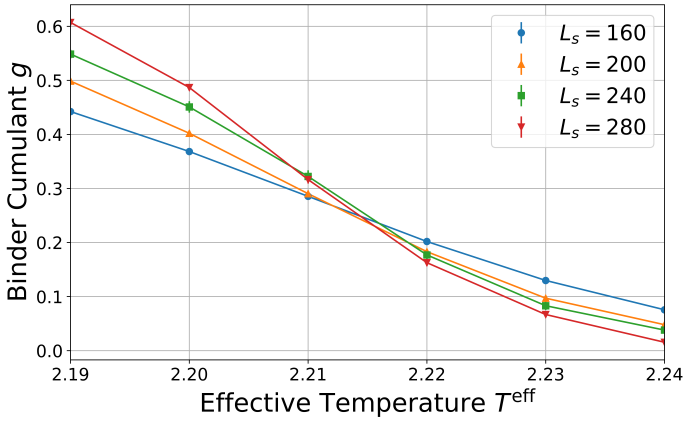

Figure 3. Binder crossing of the mapped 4D Ising model. Magnetic sites have interaction strengths $J_s = J_\tau = 1 = 100J_\perp$ and the dilution is $p = 0.1$. The sample geometry is given by $L_s = 40L_\perp$. The imaginary time size (see Sec 3.4.2) corresponds to the optimal shapes $L_\tau = L_\tau^{\max}$ (values given in Table 3). Error bars indicate statistical error over disorder configurations. The line between the data points serves as a visual aid.

A more robust method of determining the location of the critical point is based on calculating the Binder cumulant, which is defined as

$$g = \left[1 - \frac{\langle |m|^4 \rangle}{3\langle |m|^2 \rangle^2}\right]_{\text{dis}}. \tag{6}$$

At the critical temperature T_c the Binder cumulant is expected to be scale invariant, it thus takes a single value for all spatial system sizes L for a given sample shape. The quantum critical point is determined by plotting g vs. T^{eff} for all system sizes (at their respective optimal shapes, see Sec 3.4.2), and identifying the crossing point. An example of this analysis is given in Figure 3.

3.4 SAMPLE GEOMETRY

3.4.1. Effects of High Anisotropy. In the presence of strong spatial anisotropy, samples with $L_s = L_\perp$ are not ideal for the Monte Carlo simulations. This issue arises because the magnetic correlations decay much more slowly in the strongly coupled direction than in the weak directions. To address this, we adjust the aspect ratio by elongating the

Table 1. Interaction anisotropy and corresponding system size ratio. Values taken for clean system $p = 0$

$J_\perp/J_s$	$L_s/L_\perp$
0.04	2
0.033	3
0.01	5
0.001	10

lattice in the direction of strong coupling. This transformation results in a $L_s \times L_\perp \times L_\perp$ bar geometry with $L_s > L_\perp$. In the clean case, $p = 0$. we have used ratios $L_s/L_\perp$ from 2 to 10, depending on the strength of the anisotropy, as shown in Table 1. This enhances the visibility of phase transitions as the Binder crossing is roughly in the middle between $g = 0$ and $2/3$. When dilution is considered $p > 0$, the site vacancies further inhibit the magnetic interaction in the strongly coupled direction, requiring an even large scale factor to enhance the visibility of the transition. For this reason, a ratio $L_s/L_\perp = 40$ is used, for the system with a vacancy concentration $p = 0.1$ and $J_\perp = 0.01$. Note that the ratio $L_s/L_\perp$ is kept fixed as the system size is varied because both L_s and $L_\perp$ are (spatial) lengths and have the same scale dimension.

3.4.2. Imaginary Time. Generally, in the disordered system, the lengths in the spatial dimensions, L_s and imaginary time, L_τ, need to be treated as independent parameters. This comes from the fact that the disorder, which is perfectly correlated in imaginary time, but uncorrelated in space, breaks the symmetry between space and time. In disordered quantum Ising systems, correlations in space and time are expected to be related by activated scaling where the correlation length scales logarithmically with time $\xi^\psi \propto \ln(\xi_\tau)$ rather than following conventional power law scaling $\xi^z \propto \xi_\tau$. The expected activated scaling behavior leads to the finite-size scaling form

$$g_{av} = \tilde{g}_A(tL^{1/\nu}, \ln(L_\tau)/L^\psi) \tag{7}$$

. This differs from the finite-size scaling form for conventional dynamical scaling

$$g_{av} = \tilde{g}_A(tL^{1/\nu}, L_\tau/L^z). \tag{8}$$

The value of ψ (or z) is not known a priori and needs to be found together with the critical point in the simulations. An approach from Vojta et al. [11] is followed to determine the so called 'optimal' value of L_τ. This is the value, where, for a particular spatial system size L, the ratio L_τ/L roughly corresponds to the ratio of correlation lengths in time and space ξ_τ/ξ. The optimal value of L_τ is determined from analyzing the parabolic nature of the function $g_c(L_\tau)$, for constant L. This function has its maximum at position L_τ^{max} which indicates the optimal sample shape. Moreover, for samples of optimal shape ($L_\tau = L_\tau^{max}$) the value of g is independent of L at T_c^{eff}. By iteratively evaluating g_C for all L_τ considered, we can assemble a parabolic plot as is shown in Figure 4. To determine the maximum of $g_c(L_\tau)$, we perform a parabolic fit of the simulation results according to

$$g_c(L) = C - A(\ln(L) - \ln(L_\tau^{max}))^2 \tag{9}$$

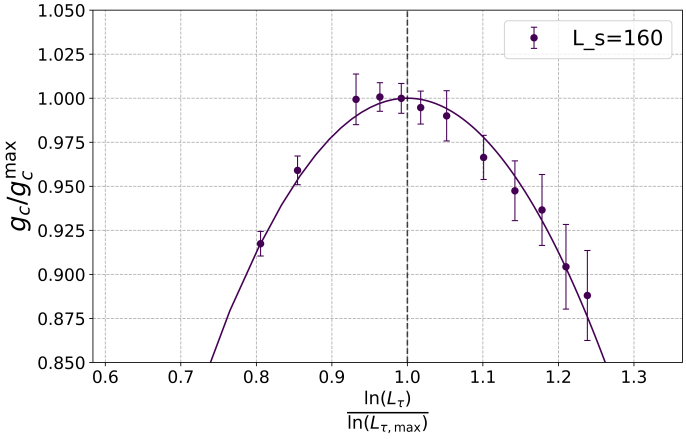

Figure 4. Binder cumulant at $T^{\text{eff}} = 2.21$, $p = 0.10$, $J_\perp = 0.01$. Error bars indicate uncertainty in g_c obtained from the standard deviation over disorder realizations. Dashed vertical line indicates maximum obtained via fitting to (9).

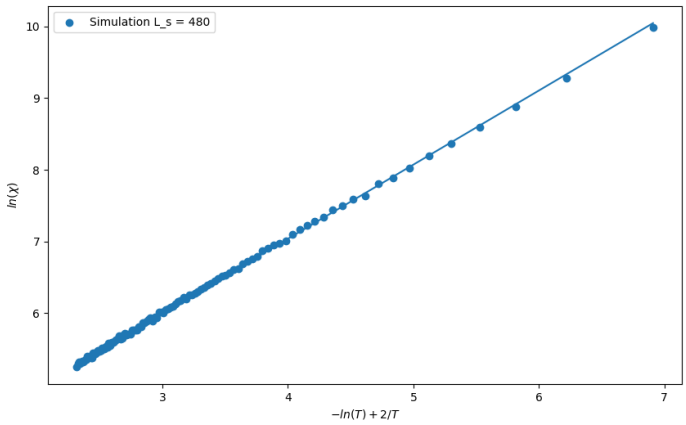

Figure 5. Calculated susceptibility $\ln(\chi)$ vs temperature $-\ln(T) + 2/T$. Straight line indicates agreement with 1D functional form (7). Clean 3D classical Ising system $p = 0$ with high anisotropy $J_s = 100J_\perp$.

where C, A and the maximum position $\ln(L_\tau^{max})$ are fitting parameters. Performing this for the set of system sizes we consider in this study, the values of $L_\tau^{\max}$ can be extracted. This is a computationally involved process that is summarized in Table 2. Note that setting L_τ to its optimal value $L_\tau^{\max}$ fixes the second argument in the scaling functions (8) and (9). The further data analysis then follows the usual one-parameter scaling in terms of tL^1/ν.

Table 2. Steps to determine critical temperature T_c and optimal shapes L_τ^{max}, see Ref [11]. sc_x is the fixed scale factor discussed in Sec. 3.4.1.

g_c vs L_τ construction
1. Select system size L: $L_\perp = L, L_s = sc_x * L$.
2. Select initial imaginary time size L_τ: $L_\tau = L_s$.
3. Select Effective Temperature Range: $T^{\mathrm{eff}} = [T_-^{\mathrm{eff}}, T_+^{\mathrm{eff}}]$.
4. Identify Critical Point: Plot g vs T^{eff} for all L. Approximate crossing occurs at g_c and T_c^{eff}.
5. Repeat: Set an increased L_τ and repeat from step 3.
6. Plotting: Plot g_c vs L_τ for each L and identify common g_c^{max} and corresponding optimal time size L_τ^{max}.

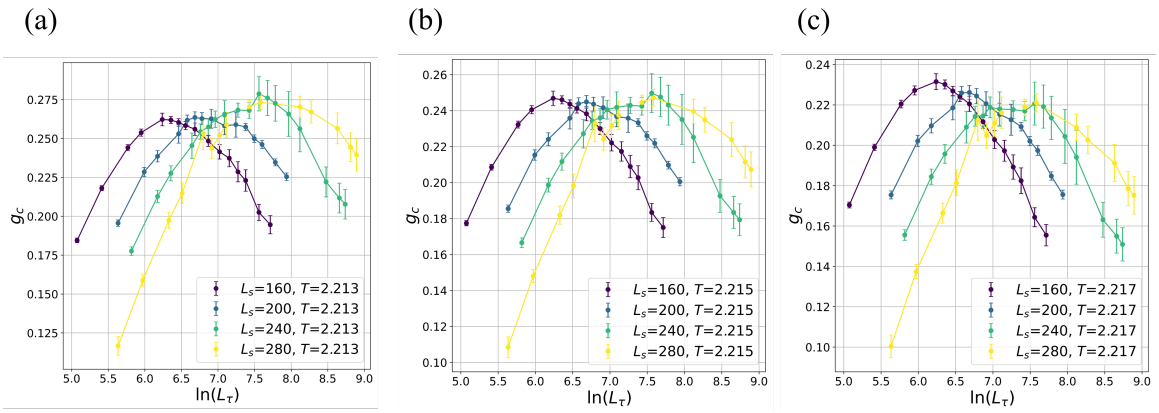

Figure 6. Binder cumulant g_c, taken with varying effective temperature, plotted for various L_τ. The dilution $p = 0.1$, with interaction strengths $J_s = J_\tau = 100J_\perp$. (a) $T < T_c$.$(b)T = T_c$. (c)$T > T_c$.

4. RESULTS

4.1 ONE-DIMENSIONAL BEHAVIOR

The magnetic interactions in cobalt niobate are highly anisotropic. We first employ the classical model (5) to verify that an anisotropy similar to the experimental one [2, 12] leads to one-dimensional behavior in the absence of dilution. To do so, we compare the calculated susceptibility for our system for different $J_\perp$ with the exact classical one-dimensional result calculated for example by Pathria [13],

$$\chi \propto \frac{1}{T}\exp(\frac{2}{T}). \tag{10}$$

Figure 5 shows the result of our simulations for $J_\perp = 0.01$, indicating an excellent agreement with the functional form for a one-dimensional Ising chain.

4.2 FINDING THE CRITICAL POINT T_c^{eff}

The critical point T_c^{eff} is determined via an iterative multi-step approach together with the optimal L_τ. For each system size L, we begin by determining the optimal values of L_τ at several temperatures around the transition, following the approaches detailed in

Table 3. Extracted optimal L_τ values for each L_s considered. $T = 2.215$, $p = 0.1$ and $J = J_\tau = 100J_\perp$.

L_s	L_τ^{max}	L_τ^{max}/L_s
160	663(6)	4.14(3)
200	1158(14)	5.79(6)
240	1750(33)	7.79(13)
280	2921(94)	10.43(31)

Sections 3.3 and 3.4.2, summarized in Table 2. The results of this analysis for the disordered quantum system are given in Figure 6. For $T^{\text{eff}} < T_c$ the maximum g of each parabola increases with increasing system size (indicating scaling towards the ordered phase), as in Figure 6a. For $T^{\text{eff}} > T_c$, in contrast, the maximum g decreases with size as the system scales towards the paramagnetic phase (Figure 6c). Right at T_c, the maximum is site-independent, as shown in Figure 6b. Based on this analysis, optimal values of L_τ at the estimated T_c^{eff} are selected for each spatial system size L, which are given in Table 3. An accurate value of T_c is then determined by identifying the crossing of the Binder cumulant curves (for the optimal shapes), with respect to temperature, for all L, as is done in Figure 3. From this analysis, the critical temperature for $p = 0.1$ and $J_\perp = 0.01$ is found to be $T_c = 2.215$

4.3 TESTING ACTIVATED SCALING

After identifying the critical point, we now turn to analyzing its critical behavior. We start with the dynamical scaling. Figure 7 shows a scaling plot of the Binder cumulant at T_c according to activated scaling (7). The parabolas for different system sizes collapse well within their error bars. In contrast, a scaling plot according to power-;aw scaling (8), does not lead to a good collapse, but the domes broaden with increasing L. This observation serves as a sign of the unconventional scaling behavior of this system. The values of the optimal L_τ in Table 3 allow us to determine the tunneling exponent ψ, considering the activated scaling relation [11]

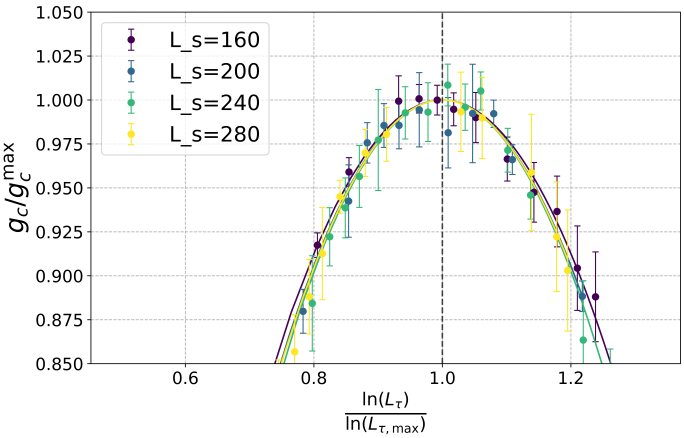

Figure 7. g_c/g_c^{max} vs $\ln(L_\tau)/\ln(L_\tau^{max})$ for multiple system sizes at the critical point $T^{\text{eff}} = 2.215$. In this study we consider ratios, of L_τ/L ranging from $1-26$, allowing the full parabolic nature of $g(L_\tau)$ to be seen. As can be seen, the parabolas collapse on one another with increasing L_s.

$$\ln(L_\tau^{max}) \propto L_s^{\psi}. \tag{11}$$

The data and fit are shown in Figure 8, yielding

$$\psi = 0.36(4). \tag{12}$$

The fit is performed via a non-linear least squares routine that returns the desired fitting parameters in addition to the covariance matrix. The square root of the diagonal elements in the covariance matrix correspond to the single standard-deviation uncertainties for each fitting parameter, indicated by the $(\ldots)$ in equation (12) for the last digits.

4.4 CORRELATION LENGTH EXPONENT

An equation for an additional critical exponent can be found by differentiating the finite-size scaling form in equation (7), with respect to T^{eff}. This yields

$$\frac{dg}{dT^{\text{eff}}} \propto L_s^{1/\nu} \tag{13}$$

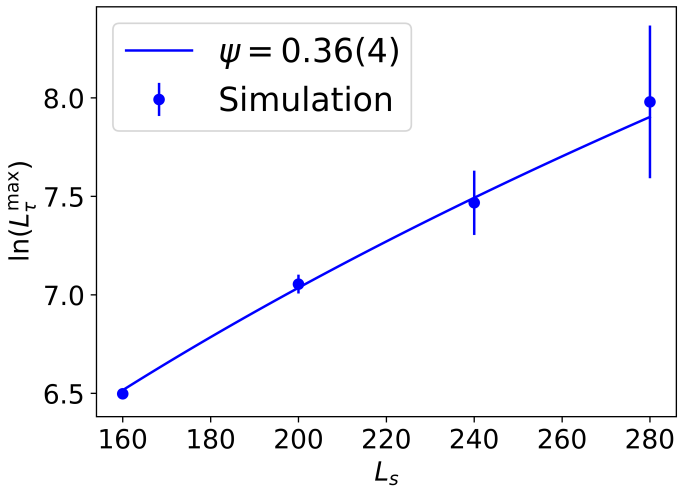

Figure 8. $\ln(L_\tau^{max})$ vs L_s^ψ taken at the critical point $T^{\text{eff}} = 2.215$. The solid line is a fit of the data with $ln(L_\tau^{\max}) = C + AL^\psi$ yielding $C = 0.3$, $A = 1$ and $\psi = 0.36(4)$.

which holds at the critical point $T^{\text{eff}} = T_c$. $\frac{dg}{dT}$ can be evaluated from the simulation data by fitting a linear dependence near the critical point. To evaluate ν, we plot $\frac{dg(L_s)}{dT^{\text{eff}}}$ versus L_s values and analyze the scaling behavior as shown in Figure 9 [2]. A fit with the power law (13) gives $1/\nu = 1.025(6)$ and consequently,

$$\nu = 0.98(2). \tag{14}$$

4.5 ORDER PARAMETER EXPONENT

To determine a complete set of critical exponents, we also consider the order parameter. The scaling behavior for the order parameter at the critical point follows from its finite-size scaling form

$$m = L_s^{\beta/\nu} \tilde{m}_A(tL^{1/\nu}, \ln(L_\tau/L^\psi)), \tag{15}$$

[2] dg/dT^{eff} is obtained via a linear fit very close to the critical point. Errors for each point are found by considering the error associated with each g value Δg. By plotting $g + \Delta g$ close to the critical point, a linear fit yields an alternative slope $d(g + \Delta g)/dT$. Error for dg/dT, $\Delta\frac{dg}{dT}$ is then taken as the difference of these slopes, $\Delta\frac{dg}{dT} = |\frac{dg}{dT} - \frac{d(g+\Delta g)}{dT}|$.

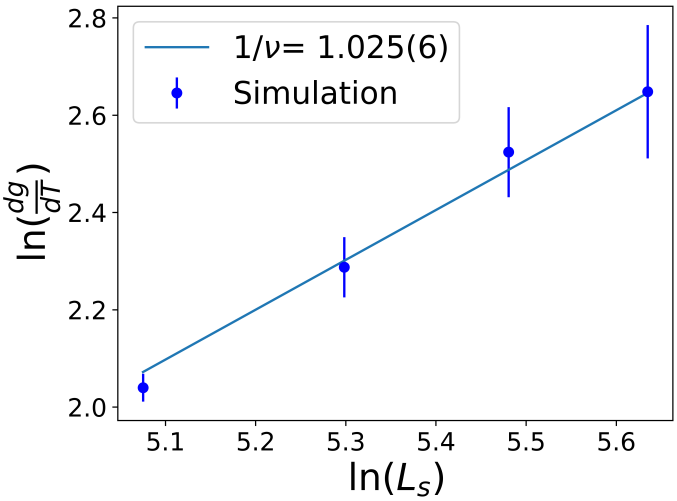

Figure 9. $\ln(\frac{dg}{dT^{\text{eff}}})$ vs $\ln(L_s)$ at the critical point $T^{\text{eff}} = T_c$. Line is a fit with equation (12). From this fit $\nu = 0.98(2)$ is extracted.

which implies the relation

$$m \propto L_s^{\beta/\nu} \tag{16}$$

at criticality, $t = 0$ and $L_\tau = L_\tau^{\max}$. Thus, we evaluate m for varying L_s at their respective optimal sizes $L_\tau(L_s)$ at the critical point. Figure 10 shows a plot of this result, where a fit corresponding to equation (15) is performed. This analysis yields, $\frac{\beta}{\nu} = 1.94(12)$, which gives from equation (13),

$$\beta = 1.89(11). \tag{17}$$

4.6 DISCUSSION

To identify the universality class of the quantum phase transition studied in this work, we compare our calculated critical exponents with those obtained in previous work for the disordered transverse-field Ising model in three dimensions. We also compare with the three-dimensional disordered contact process which is expected to be in the same universality class.

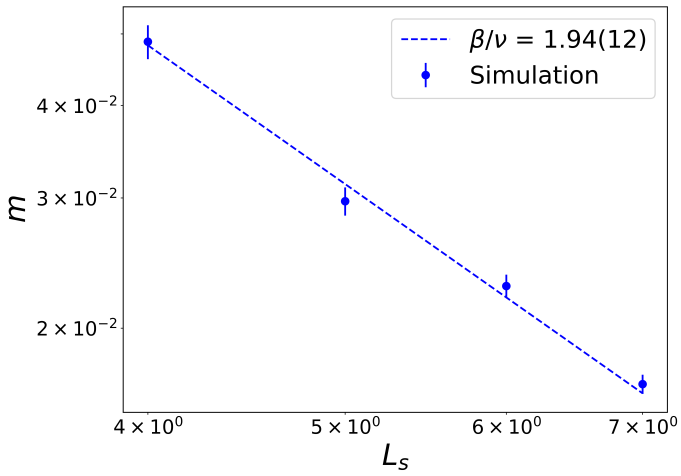

Figure 10. Order parameter m vs L_s at the critical point $T^{\text{eff}} = T_c$. The line is a fit with (15) from which $\beta/\nu = 1.94(12)$ is extracted. Error bars indicate calculated uncertainty over disorder realizations. Both axes are on a logarithmic scale.

The critical exponents calculated for our system are in good agreement with those found in previous work for 3D systems as shown in Table 4. They however, do not agree with the exponents of the 1D-TFIM observed for the pure system. Thus, we have demonstrated that the critical behavior of the site-diluted, strongly anisotropic quasi-1D Ising model belongs to the same universality class as that of the generic disordered 3D transverse-field Ising model.

Table 4. Critical exponents for the site diluted quasi-one-dimensional transverse-field Ising model (this work) compared to the 3D disordered contact process [14], strong-disorder renormalization group prediction for the 3D transverse-field Ising model [15], and 1D transverse-field Ising model [16].

Source	ψ	ν	β
This Work	0.36(4)	0.98(2)	1.89(11)
Ref [14]	0.38(3)	0.98(6)	1.87(7)
Ref [15]	0.46(2)	0.99(2)	1.82(4)
Ref [16]	1/2	2	(3-$\sqrt{5}$)/2

5. CONCLUSIONS

In this paper, we constructed a simple model to characterize the magnetic quantum phase transition of cobalt niobate with magnetic site dilution. We execute this by considering a $3D$ transverse-field Ising model, with high spatial anisotropy, that we map to a 4D classical Ising model. Through Monte Carlo simulations, we are able to analyze the magnetic properties at the quantum critical point and study this transition and its scaling behavior.

The transition is analyzed by calculating various thermodynamic quantities at the critical point. Using finite-size scaling, we study the variation of these quantities with both the spatial length and imaginary time length of the sample. The results indicate unconventional scaling associated with an infinite-randomness fixed point. By utilizing activated scaling relations, we calculate three critical exponents that describe the universality class of the transition in our system. We find that the critical exponents agree excellently with those published in the literature for the disordered 3D transverse-field Ising universality class.

This is an interesting result, particularly in view of the observation of 1D critical behavior in the clean undiluted cobalt niobate. We emphasize that the behavior corresponding with the one-dimensional TFIM observed in experiment, does not translate well to the disordered system due to the inability to establish long-range magnetic order along the chains in the presence of vacancies. Our results confirm the notion that long-range order in the diluted system crucially depends on the weak interchain interactions and is thus intrinsically three-dimensional. We hope that this work inspires further experiments into diluted cobalt niobate, such that the predictions made here can be tested.

REFERENCES

[1] Anubhav Jain, Shyue Ping Ong, Geoffroy Hautier, Wei Chen, William Davidson Richards, Stephen Dacek, Shreyas Cholia, Dan Gunter, David Skinner, Gerbrand Ceder, and Kristin A. Persson. Commentary: The Materials Project: A materials genome approach to accelerating materials innovation. *APL Materials*, 1(1):011002, 07 2013.

[2] R. Coldea, D. A. Tennant, E. M. Wheeler, E. Wawrzynska, D. Prabhakaran, M. Telling, K. Habicht, P. Smeibidl, and K. Kiefer. Quantum criticality in an ising chain: Experimental evidence for emergent e¡sub¿8¡/sub¿ symmetry. *Science*, 327(5962):177–180, 2010.

[3] Robert C. Pullar. The synthesis, properties, and applications of columbite niobates (m2+nb2o6): A critical review. *Journal of the American Ceramic Society*, 92(3):563–577, 2009.

[4] Subhash Thota, Sayandeep Ghosh, Maruthi R, Deep C. Joshi, Rohit Medwal, Rajdeep S. Rawat, and Mohindar S. Seehra. Magnetic ground state and exchange interactions in the ising chain ferromagnet $Conb_2o_6$. *Phys. Rev. B*, 103:064415, Feb 2021.

[5] C. M. Morris, Nisheeta Desai, J. Viirok, D. Hüvonen, U. Nagel, T. Rõõm, J. W. Krizan, R. J. Cava, T. M. McQueen, S. M. Koohpayeh, Ribhu K. Kaul, and N. P. Armitage. Duality and domain wall dynamics in a twisted kitaev chain. *Nature Physics*, 17(7):832–836, April 2021.

[6] R. J. Elliott, P. Pfeuty, and C. Wood. Ising model with a transverse field. *Phys. Rev. Lett.*, 25:443–446, Aug 1970.

[7] Subir Sachdev. *Quantum Phase Transitions*. Cambridge University Press, 2 edition, 2011.

[8] Thomas Vojta. Phases and phase transitions in disordered quantum systems. *AIP Conference Proceedings*, 1550(1):188–247, 08 2013.

[9] Ulli Wolff. Comparison between cluster monte carlo algorithms in the ising model. *Physics Letters B*, 228(3):379–382, 1989.

[10] Nicholas Metropolis, Arianna W. Rosenbluth, Marshall N. Rosenbluth, Augusta H. Teller, and Edward Teller. Equation of state calculations by fast computing machines. *The Journal of Chemical Physics*, 21(6):1087–1092, 06 1953.

[11] Thomas Vojta and Rastko Sknepnek. Quantum phase transitions of the diluted o(3) rotor model. *Phys. Rev. B*, 74:094415, Sep 2006.

[12] J. Larsen, T. Schäffer, Ursula Hansen, Sonja Holm-Dahlin, S. Ahl, Rasmus Toft-Petersen, J. Taylor, G. Ehlers, Jens Jensen, Henrik Ronnow, Kim Lefmann, and N. Christensen. Spin excitations and quantum criticality in the quasi-one-dimensional ising-like ferromagnet cocl 2 · 2 d 2 o in a transverse field. *Physical Review B*, 96, 11 2017.

[13] R.K. PATHRIA. *CHAPTER 12 - PHASE TRANSITIONS: EXACT (OR ALMOST EXACT) RESULTS FOR THE VARIOUS MODELS*. Butterworth-Heinemann, Oxford, second edition edition, 1996.

[14] Thomas Vojta. Monte carlo simulations of the clean and disordered contact process in three dimensions. *Phys. Rev. E*, 86:051137, Nov 2012.

[15] István A. Kovács and Ferenc Iglói. Infinite-disorder scaling of random quantum magnets in three and higher dimensions. *Phys. Rev. B*, 83:174207, May 2011.

[16] Daniel S. Fisher. Critical behavior of random transverse-field ising spin chains. *Phys. Rev. B*, 51:6411–6461, Mar 1995.

SECTION

2. CONCLUSIONS

This work details an investigation into the effects of site dilution and anisotropy on the critical behavior of varying Ising systems. Beginning from a simple one-dimensional classical Ising chain, systems of increasing complexity are studied, up to a three-dimensional disordered quantum Ising system. The principles developed here are then applied towards modeling the quantum phase transition of diluted cobalt niobate. The following paragraphs will summarize this work and our findings.

In the first section, the magnetic phase transitions of the classical one- and two-dimensional Ising systems, with periodic boundary conditions, are evaluated, where we validate Ising and Onsager's exact solutions, respectively. To facilitate the investigation of more complex systems, such as those in three dimensions, Monte Carlo methods are introduced, which are used consistently through the remainder of this work to obtain approximate solutions of the critical points. Quenched disorder is then introduced in the form of random site dilution (i.e. randomly placed vacancies that are substituted for magnetic sites). The significant effects of the disorder on the system are then illustrated through the construction of the magnetic phase boundary for the diluted three-dimensional classical Ising system, and the Harris criterion is employed to study its influence on critical points. Finally, what is learned is applied to the transverse-field Ising model, laying the groundwork for studying quantum phase transitions.

In Paper I, we propose a model to allow for the investigation into the quantum critical behavior of the disordered cobalt niobate magnetic system. Such a model, is constructed from a disordered three-dimensional transverse-field Ising model that is mapped onto a four-dimensional classical Ising system for numerical efficiency. The spatial anisotropy

observed in experiments for this system is implemented via one-dimensional chains of strongly coupled magnetic sites that are weakly connected in the remaining two directions. The magnetic properties for systems of varying sizes are characterized and measured close to the quantum phase transition via large-scale Monte Carlo simulations. The scaling behavior of the magnetic quantities close to the quantum critical point is studied. A trio of critical exponents is extracted, which are used to determine the universality class for the quantum phase transition. An unconventional activated scaling relation is discovered, characterized by a tunneling exponent $\psi = 0.36(4)$. This implies that the quantum critical point is of infinite-randomness type. We additionally determine the values for the correlation length exponent $\nu = 0.98(2)$ and order parameter exponent $\beta = 1.89(11)$. This set of critical exponents, as shown in Table 4, are in good agreement with previously obtained values from literature for the three-dimensional disordered contact process [17] and three-dimensional transverse-field Ising model [18].

In summary, this work gives an introduction to the Ising model and how it is used to model magnetic phase transitions for a variety of systems. Beginning with variations to the systems dimensionality, increasingly complex modifications are made incorporating anisotropy, disorder, and quantum effects. All three of these complications, are exhibited by disordered cobalt niobate, which we present a model and analysis for here. This work illustrates the diverse range of solutions and behavior for Ising models and should motivate additional investigations into the fascinating critical behavior exhibited by systems that couple disorder and anisotropy.

REFERENCES

[1] Clarke, J.B., Hastie, J.W., Kihlborg, L.H.E., Metselaar, R. and Thackeray, M.M., 1994. Definitions of terms relating to phase transitions of the solid state (IUPAC Recommendations 1994). Pure and Applied Chemistry, 66(3), pp.577–594.

[2] Gallavotti, G., 1999. *Statistical Mechanics, Short Treatise*. Springer-Verlag, Berlin, 1st edition.

[3] Nolting, W. and Ramakanth, A., 2009. Exchange interaction. In *Quantum Theory of Magnetism*, Springer, Berlin, Heidelberg, pp.175–231.

[4] Landau, L.D. and Lifshitz, E.M., 1980. *Statistical Physics*, Course of Theoretical Physics, Vol. 5. Butterworth-Heinemann, Oxford, 3rd edition.

[5] Wolschin, G., 2021. Statistical physics of phase transitions. Lecture Notes. (Accessed: 2024-09-07).

[6] Pathria, R.K., 1996. CHAPTER 13 – PHASE TRANSITIONS: The Renormalization Group Approach. In *Statistical Mechanics (Second Edition)*, Butterworth-Heinemann, Oxford, pp.414–423.

[7] Lewis, A.S., 1996. Group invariance and convex matrix analysis. SIAM Journal on Matrix Analysis and Applications, 17(4), pp.927–949.

[8] Pathria, R.K., 1996. CHAPTER 12 – PHASE TRANSITIONS: Exact (or Almost Exact) Results for the Various Models. In *Statistical Mechanics (Second Edition)*, Butterworth-Heinemann, Oxford, pp.366–413.

[9] Onsager, L., 1944. Crystal statistics. I. A two-dimensional model with an order-disorder transition. Physical Review, 65(3-4), pp.117–149.

[10] Kaufman, B. and Onsager, L., 1949. Crystal statistics. III. Short-range order in a binary Ising lattice. Physical Review, 76(8), pp.1244–1252.

[11] Metropolis, N., Rosenbluth, A.W., Rosenbluth, M.N., Teller, A.H. and Teller, E., 1953. Equation of state calculations by fast computing machines. The Journal of Chemical Physics, 21(6), pp.1087–1092.

[12] Binder, K. and Heermann, D.W., 2010. *Monte Carlo Simulation in Statistical Physics: An Introduction*. Springer Berlin Heidelberg.

[13] Wolff, U., 1989. Comparison between cluster Monte Carlo algorithms in the Ising model. Physics Letters B, 228(3), pp.379–382.

[14] Sowadski, L., Anderson, S., Lerch, C., Medvedeva, J. and Vojta, T., 2024. Magnetic properties of diluted hexaferrites. Physical Review B, 110(1), p.014432.

[15] Wang, J., Zhou, Z., Zhang, W., Garoni, T.M. and Deng, Y., 2013. Bond and site percolation in three dimensions. Physical Review E, 87(5), p.052107.

[16] Cardy, J., 1996. *Scaling and Renormalization in Statistical Physics*. Cambridge University Press, Cambridge.

[17] Harris, A.B., 1974. Effect of random defects on the critical behaviour of Ising models. Journal of Physics C: Solid State Physics, 7(9), p.1671.

[18] Vojta, T., 2013. Phases and phase transitions in disordered quantum systems. AIP Conference Proceedings, 1550(1), pp.188–247.

[19] Vojta, T., 2006. Rare region effects at classical, quantum and nonequilibrium phase transitions. Journal of Physics A: Mathematical and General, 39(22), p.R143.

[20] Fisher, D.S., 1995. Critical behavior of random transverse-field Ising spin chains. Physical Review B, 51(10), pp.6411–6461.

[21] Vojta, T., 2012. Monte Carlo simulations of the clean and disordered contact process in three dimensions. Phys. Rev. E, 86(5), p.051137.

[22] Kovács, I. A. and Iglói, F., 2011. Infinite-disorder scaling of random quantum magnets in three and higher dimensions. Phys. Rev. B, 83(17), p.174207.

VITA

Logan Sowadski was born at St. Luke's Hospital in St. Louis on the 23rd of October, 2001. He began his studies at St. Louis Community College in 2018, transferring to the Missouri University of Science and Technology in 2020. He joined Dr. Thomas Vojta's research group in 2022. He received his Bachelor's of Science in Physics in 2023, beginning his Master's of Science the same year. In July 2025, he received his Master of Science degree in Physics from the Missouri University of Science and Technology.